Beam Stability and Optics Studies of the CNGS Transfer Line

J. Wenninger, V. Kain, M. Meddahi

Abstract

Optics and stability of the CNGS transfer lines TT40 and TT41 were studied with beam trajectories during its commissioning in July and August 2006. Steering magnet response measurements were used to analyze the optics and the quality of the steering magnets and of the beam position monitors. A strength error of the main quadrupoles was identified with this technique and corrected during the commissioning. The dispersion was measured and found to be close to the nominal value. Finally the short and the long term stability of the transfer lines were studied. The transfer line was found to be very stable and the dominant source of short term position jitter is due to the ripple of the extraction septum and energy fluctuations in the SPS.

Geneva, Switzerland

January 25, 2007

1   Introduction

The SPS extraction in LSS4, the TT40 and TT41 transfer lines were commissioned for CNGS beam operation in July and August 2006 in three periods of one week. A large fraction of the beam time was devoted to studies of the line optics, aperture and stability. At the end of the third commissioning week regular operation of the CNGS transfer lines started for a two week period.

   This note begins with a short description of the first steering and of the major adjustments that had to be made for steering and for the momentum. Response data results are then presented, followed by an analysis of the dispersion of the transfer line. Finally an analysis is performed on the short and long term stability of the transfer line.

2   Steering to Target

The first low intensity beam reached the beam screen in front of target T40 without any steering in the TT41 transfer line indicating a good alignment of the line elements.

   Due to problems with the auto-trigger system of the beam position monitors (BPMs), the first steering was performed on 11th July using OTR beam screen data. The largest error was found to originate from the strong MBSG.4100 dipole string that deflects the beam horizontally towards the TT41 transfer line. The angle of each of the 8 magnets had to be corrected by $+28\mu rad$ from -3.125 to -3.152 mrad. Figure 1 shows the first trajectory recorded with the beam screens and the same trajectory after correction of the MBSG error and some orthogonal steering in front of the target.

   After the initial steering with screens, the first complete trajectory was recorded with the BPMs on 13th July. This trajectory is shown in Figure 2 together with the corrected trajectory that was used as reference for the CNGS pilot run.

   Initially the reference momentum for TT40 and TT41 was set to 399.2 GeV/c for a nominal SPS beam momentum of 400 GeV/c. This correction corresponds to the same relative SPS momentum error at 400 GeV/c as at 450 GeV/c where an accurate calibration of the momentum was performed in 2002 with Lead ion beams [1]. The first trajectory measurements with BPMs shown in Figure 2 revealed that the momentum setting of TT41 was still too high. The nominal momentum of TT40 and TT41 had to be reduced to 398.5 GeV/c to match the momentum of the extracted SPS beam. This setting is consistent with a momentum estimate of 398.2 ± 0.2 GeV/c obtained from the SPS reference magnet NMR probes. The consistency of those values indicates that the calibration of the TT41 main dipoles is accurate up to a few 10^{-4} [2].

   A relative momentum difference of 10^{-4} was observed systematically between the two extracted batches. This is most likely to due to a small difference of the main dipole field of the SPS ring. Indeed over the very short CNGS flat top the main power converter current is not constant.

3   Response Measurements

The observation of the trajectory response to controlled dipole corrector magnet deflections is a simple, yet powerful method to gain insight into the optics model of a ring or of a transfer line [3,
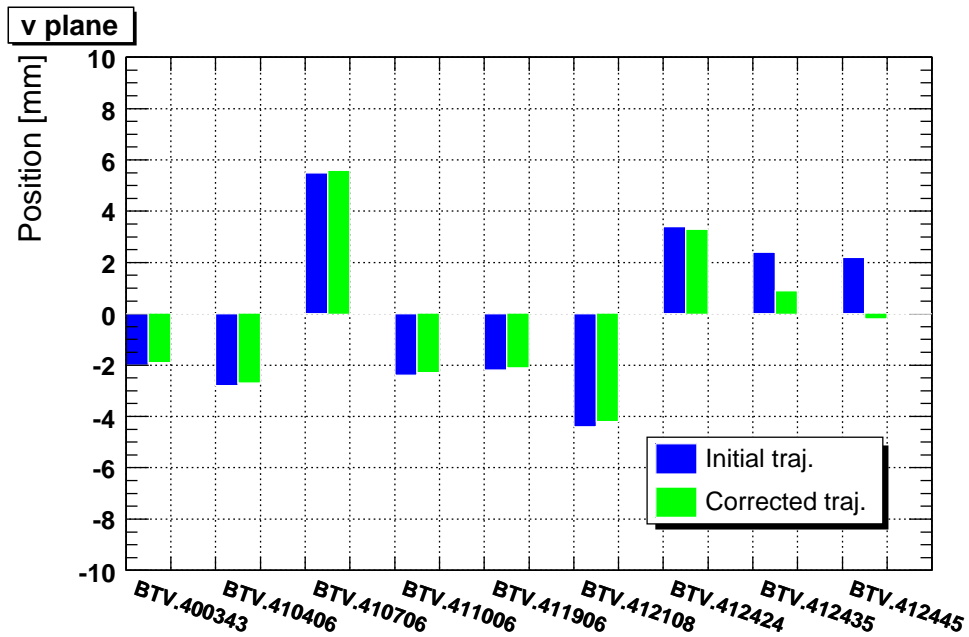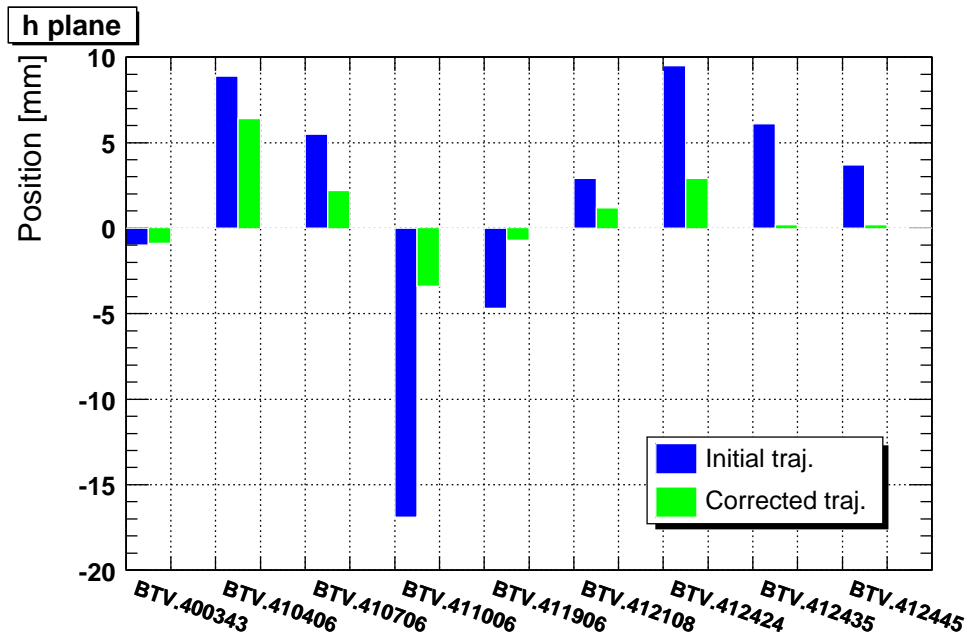
Figure 1: Horizontal (top) and vertical (bottom) trajectory in the TT40 and TT41 line recorded on 11th July by the beam screens for the very first extraction to the target and after correction of the main error due to MBSG.4100 dipole string and orthogonal steering in front of the target. Target T40 is on the right.
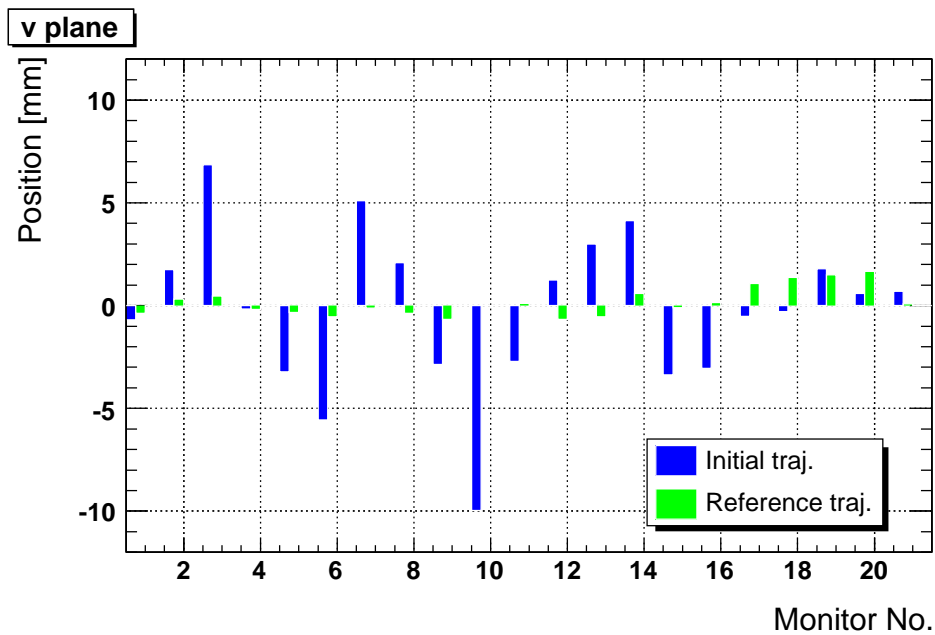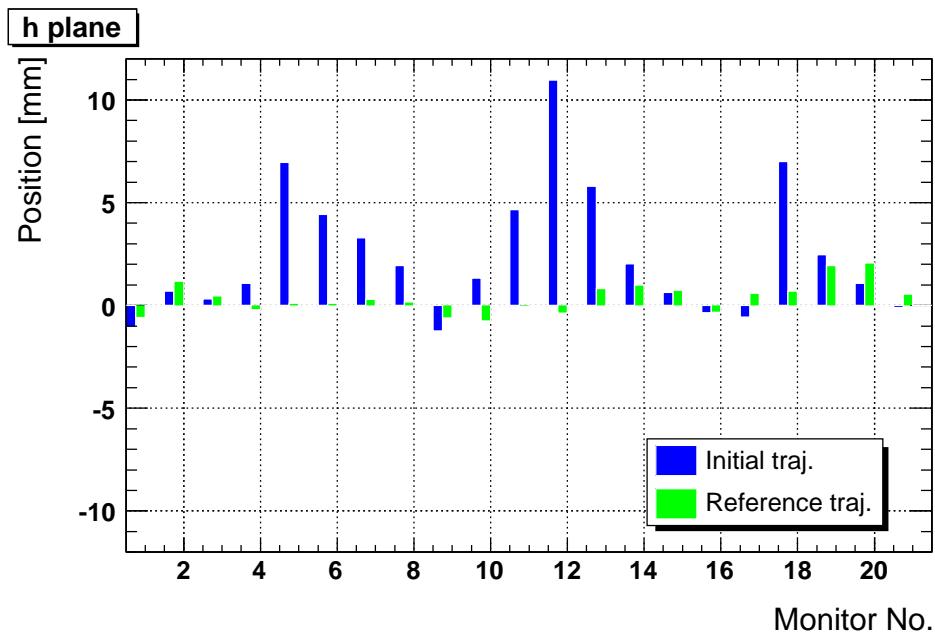
3

Figure 2: Horizontal (top) and vertical (bottom) trajectory in the TT40 and TT41 line measured by the beam position monitors for the first measured trajectory (by the BPMs) and for the reference trajectory used during the CNGS pilot run. The first horizontal trajectory reveals an energy mismatch between the extracted SPS beam and the transfer line: the extracted beam momentum is too low by ~ 1.7 permill.

4]. From a systematic measurement of the response for each corrector magnet information can be obtained on the optics model, beam position monitor quality and orbit corrector calibrations with an appropriate data analysis. At the SPS response measurements and optics verifications have been performed successfully for the SPS ring [4], the TT10 transfer line and the TI8 transfer line [5].

3.1 Optics Errors

A first response measurement involving all corrector magnets was performed during the first CNGS commissioning week. The typical r.m.s. BPM noise for the measurements was 100 μm in the horizontal and 40 to 50 μm in the vertical plane. The origin of the noise difference is explained in section 5. A fit of this data set using only corrector strengths and BPM calibration factors as free fit parameters, i.e. with a fixed nominal optics, resulted in large fit residuals and revealed optics problems that were mostly apparent towards the end of the TT41 transfer line as can be seen in Figure 3. Repeating the fit with quadrupole strengths as additional free parameters indicated a systematic strength error of the main QF (QTGF4104M) and QD (QTGD4103M) quadrupole strings. The results of the fit strengths are shown in Table 1. The strength errors reached +1.2% for the QF and +1.5% for the QD string.

Following this observation the strength setting of the two strings were changed by $\Delta K_{QF} = -0.0019$ m^{-2} and by $\Delta K_{QD} = +0.0037$ m^{-2} at the beginning of the third commissioning week. Following this change a new measurement and fit sequence indicated that the corrected strength were more or less consistent with the nominal values (see Table 1). Figure 4 gives an example of response data fit after the adjustment of the QD and QF strings.

Table 2 compares the results of two fits to the response data acquired in the third week after the change of the main quadrupole strengths discussed above. A first fit (No. 1) uses only the QF and QD strengths as free parameters, while the second fit (No. 2) uses 8 additional matching quadrupole strengths. It is of course not surprising that adding more free fit parameters improves the fit quality, but the residual error between data and fit model is reduced strongly in the vertical plane for fit No. 2. For this fit the horizontal and vertical plane residuals (r.m.s. difference data-model) are close to the values expected from the measurement noise. It is interesting to note that with one exception (QTL4122) all fit strengths are larger than nominal. Unfortunately it is very difficult to judge which of the strength changes observed with fit No. 2 correspond to real errors and which ones are due to measurement noise because the differences are very small and close to the noise level. The dispersion data that is presented in the following section will give an independent indication that some of the results of fit No. 2 may actually correspond to real errors.

The influence of the model errors on the betatron function at target T40 has been evaluated for different fits. After correction of the QD and QF strengths, the change of the betatron functions at the target for different fits did not exceed ±0.5 m in the horizontal ($\beta_{nom} = 10$ m) and ±2 m in the vertical plane ($\beta_{nom} = 20$ m). The predicted beta-beat never exceeds ± 10%, which is perfectly acceptable. Figure 5 shows the beta-beat induced by the strengths obtained from Fit No.2 of Table 1. It must be noted that this beta-beat does **not** include errors coming from the initial conditions (i.e. from the SPS ring).

5

Measurement	K_{QF} (m^{-2})	K_{QD} (m^{-2})
Nominal	0.02019	-0.02087
Week No. 1 fits	0.02044 $\pm$ 0.0004	-0.02118 $\pm$ 0.0004
Week No. 3 fits	0.02027 $\pm$ 0.0004	-0.02089 $\pm$ 0.0004

Table 1: Strength of the main quadrupole strings K_{QF} (QTGF4104M) and K_{QD} (QTGD4103M) for fits performed on data collected in the first and in the third commissioning week (after adjustment of both strengths). The strength errors indicate the range of variation for different fit assumptions and combinations of free parameters.

Fit Strength		Fit No. 1	Fit No. 2	Nominal
QD	(m^{-2})	-0.02092	-0.02085	-0.02087
QF	(m^{-2})	0.02030	+0.02024	+0.02019
QTLD.4101	(m^{-2})	-	-0.01466	-0.01436
QTGF.4102	(m^{-2})	-	+0.02095	+0.02086
QTDG.4117	(m^{-2})	-	-0.02148	-0.02123
QTGF.4118	(m^{-2})	-	+0.02575	+0.02528
QTDG.4119	(m^{-2})	-	+0.02682	+0.02632
QTDG.4121	(m^{-2})	-	-0.00790	-0.00717
QTL.4122	(m^{-2})	-	-0.01057	-0.01060
Fit Parameter				
Horizontal residual	(μm)	160	150	-
Vertical residual	(μm)	165	80	-
χ^2		2143	273	-

Table 2: Comparison of two fits of the response data from the third commissioning week (15th August 2006). For fit No. 1 only the strength of the main F and D quadrupole strings (K_{QD} and K_{QF}) were used as free parameters in addition to monitor and corrector calibrations. For fit No. 2 the strengths of 8 additional individually powered matching quadrupoles were allowed to vary freely, yielding an improved fit quality for the vertical plane. The fit residual is the r.m.s. difference between data and model after fit. The residuals expected from the noise are $\simeq 150\ \mu$m for the horizontal and $\simeq 75\ \mu$m in the vertical plane.

3.2 BPM Calibration

It is not possible from the response data alone to define the absolute calibration of BPMs and correctors. On the other hand, assuming that the average calibration of the steering magnets is correct, the response data indicates that the BPM scale is systematically too low by 7% in both planes, i.e. on average the reading of the BPMs must be multiplied by a factor 1.07. The spread of the calibration factor is 7%. For BPM BPG.4122 a cabling error was detected by the fit: the horizontal and vertical plane cables had been mixed together.
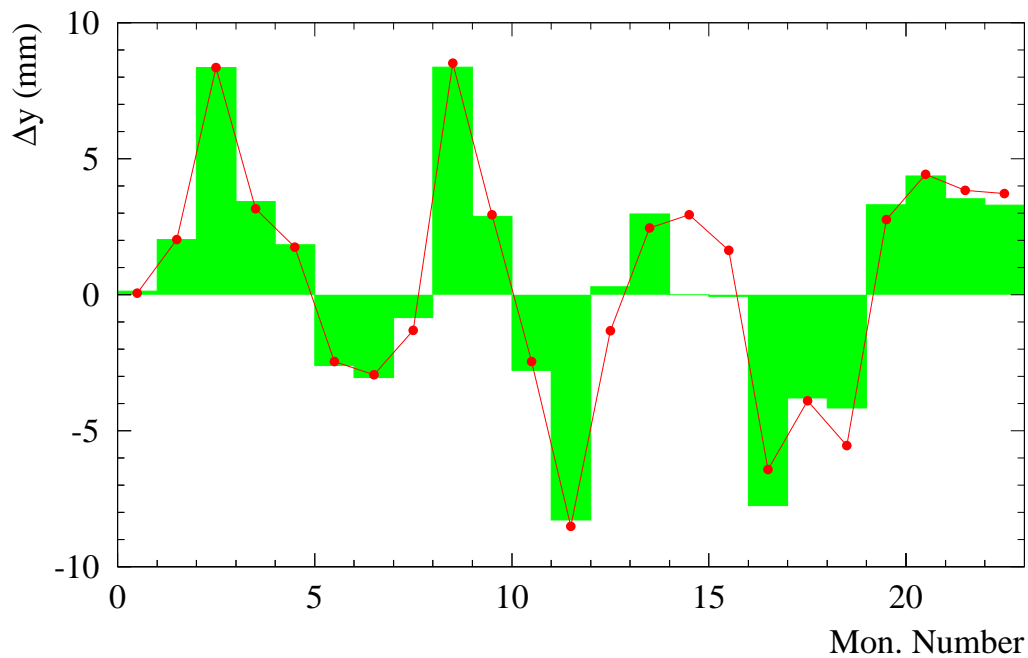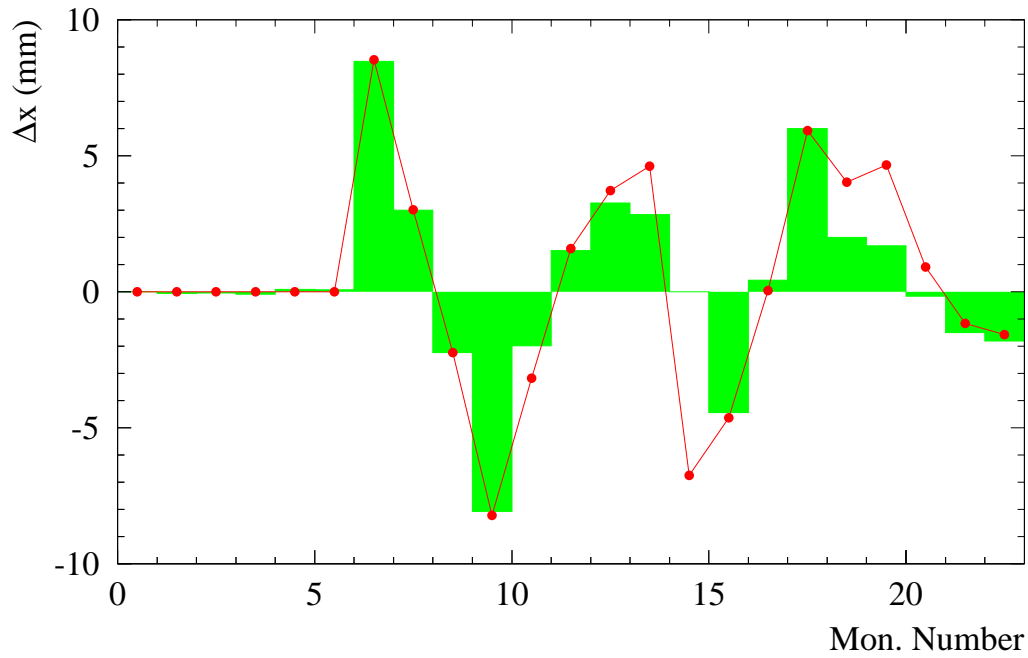
Figure 3: Example of response data for the horizontal (top, corrector MDGH.4102) and for the vertical plane (bottom, MDMV.4000). The histogram represents the data corrected by calibration factors, while the line and points correspond to the model response after fit. Monitor no. 14 did not return any data. In this case the quadrupole strengths have not been used in the fit, only corrector and monitor calibration factors were adjusted. The model corresponds therefore to the nominal optics. The discrepancy between data and model in the last part of the line is clearly visible.

7
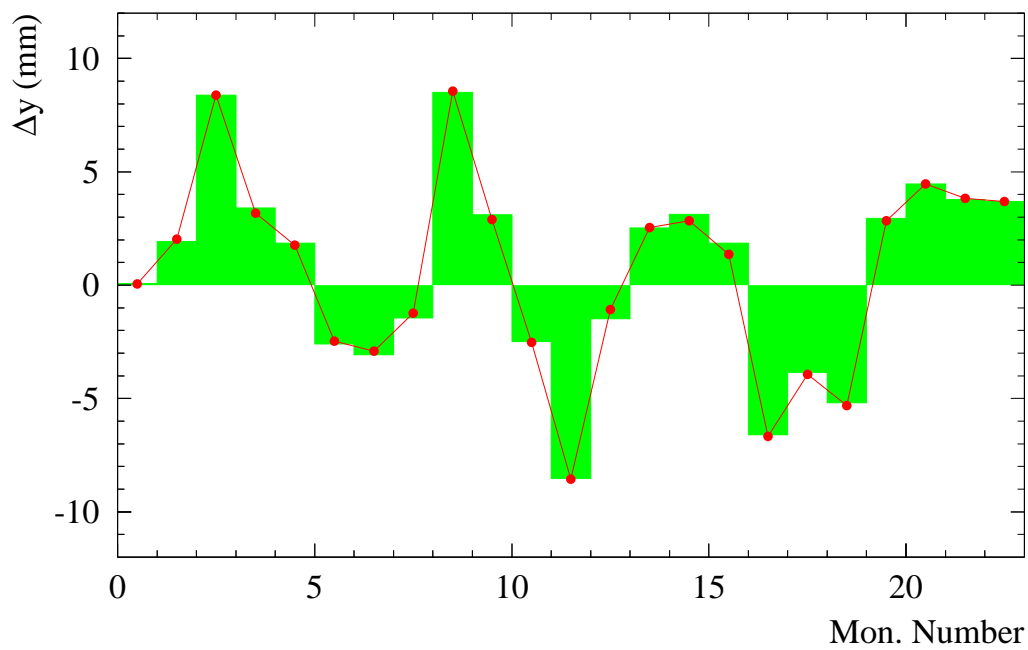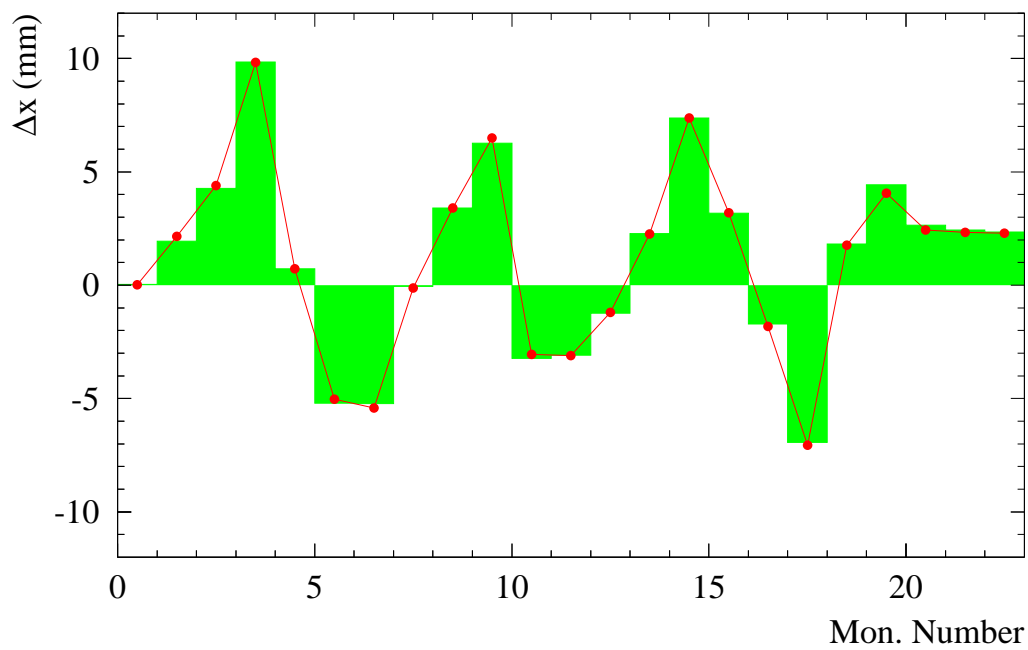
Figure 4: Example of response data for the horizontal (top, MDHC.4001) and for the vertical plane (bottom, MDMV.4000) after adjustment of the main quadrupole strength. The histogram represents the data corrected by calibration factors, while the line and points correspond to the model response after fit.
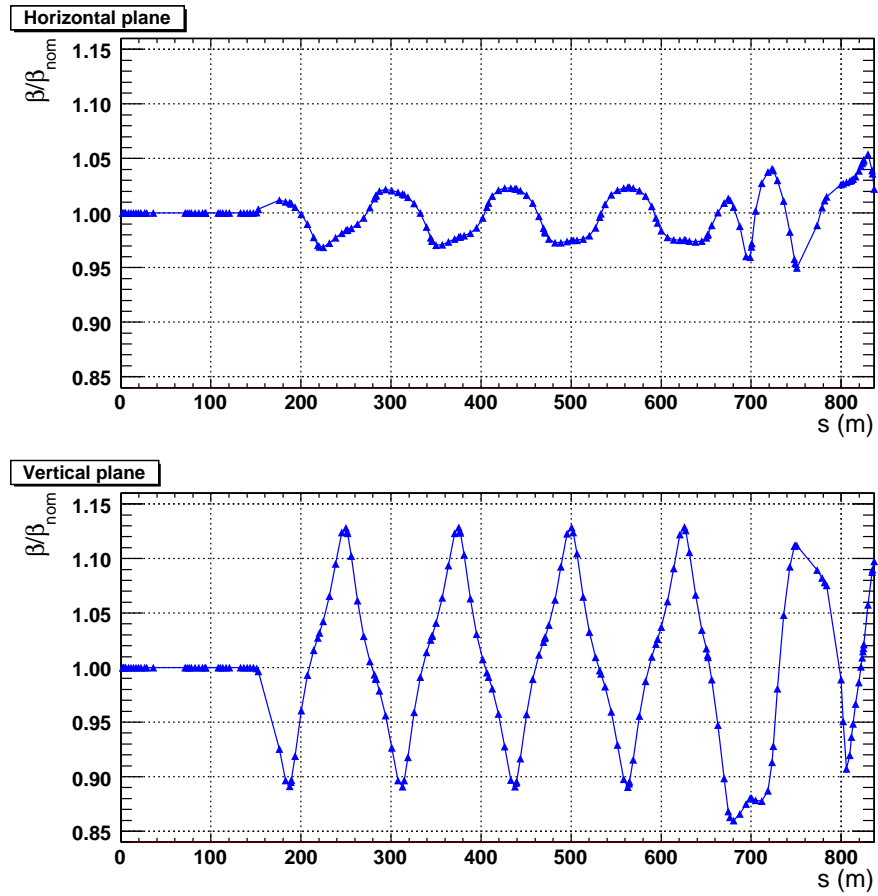
8

Figure 5: Beta-beating in TT40 and TT41 (with respect to the nominal optics) as a function of the longitudinal coordinate for the model corresponding to fit No. 2. of Table 2.

4 Dispersion

The dispersion was measured by recording the trajectory in TT40 and TT41 as a function of the beam momentum in the SPS. The beam momentum of the SPS was changed by radial steering (RF frequency change) over an interval of $\pm 0.125\%$. The dispersion was determined for each BPM individually by a fit of the position versus momentum offset in the SPS. Within the selected range the fits were always linear within the estimated measurement errors.

The dispersion was fitted assuming that the dispersion error is due entirely to an error on the initial conditions, i.e. the origin is in the SPS ring. Under those assumptions the dispersion error $\Delta D(s)$ follows a simple betatron oscillation and can be expressed as

$$\frac{\Delta D(s)}{\sqrt{\beta(s)}} = \left(\frac{\alpha_0 \, \Delta D_0}{\sqrt{\beta_0}} + \sqrt{\beta_0} \, \Delta D_0' \right) \sin \mu(s) + \frac{\Delta D_0}{\sqrt{\beta_0}} \cos \mu(s) \qquad (1)$$

$$= C \sin(\mu(s) + \phi) \qquad (2)$$

where the constants ΔD_0 and $\Delta D_0'$ are the errors on the initial dispersion and dispersion derivative. β, μ and α refer to the usual twiss parameters. Index $'0'$ refers to the start of the line $(s = 0)$. The constant C is useful to estimate the maximum possible dispersion error at a given point, namely $\Delta D_{max}(s) = C\sqrt{\beta(s)}$.

The fit results presented here refer to the transfer line optics after correction of the main quadrupole errors described in Section 3. The calibration of the BPMs, with an average scale factor of 1.07, is taken into account in the fit. The momentum error estimate obtained from the SPS BPMs is corrected by a factor 1.1 to take into account the scale error of the SPS BPMs. The momentum and BPM calibration scales almost compensate each other. If the correction factor of 1.1 for the momentum scale is not taken into account, the dispersion cannot be fitted and the data looks partly un-physical.

Figure 6 and 7 present the fit of the normalized dispersion error $(D_{meas} - D_{model})/\sqrt{\beta}$ as a function of the nominal phase advance. For Figure 6 the transfer line optics corresponds to fit No. 1 of Table 2, for Figure 7 to fit No. 2. The dispersion fit quality is approximately 30% better for the model from fit No. 2. This may be an independent indication that the results of this fit correspond to a real error and are not produced by measurement noise. In the horizontal plane the errors on initial conditions range between 1 and 3 cm for ΔD_0 and between -5 and -8 mrad for $\Delta D_0'$. For the vertical plane the errors are small: ΔD_0 is consistent with zero and $\Delta D_0'$ is approximately 0.4 to 0.5 mrad.

The measured dispersion is shown together with the fit result in Figures 8 and 9. The agreement is good all along the line, but for the horizontal plane the better match of fit No. 2 is visible. The main effect of the dispersion error is the introduction of a non-zero dispersion at the target T40 in the horizontal plane. The residual dispersion is 8 to 10 cm in the horizontal and 3 to 5 cm in the vertical plane.

As a side outcome of one of the dispersion measurements, the momentum aperture of the transfer line was determined to be +0.9% for positive momentum offsets. The aperture limit for negative offsets was not measured.
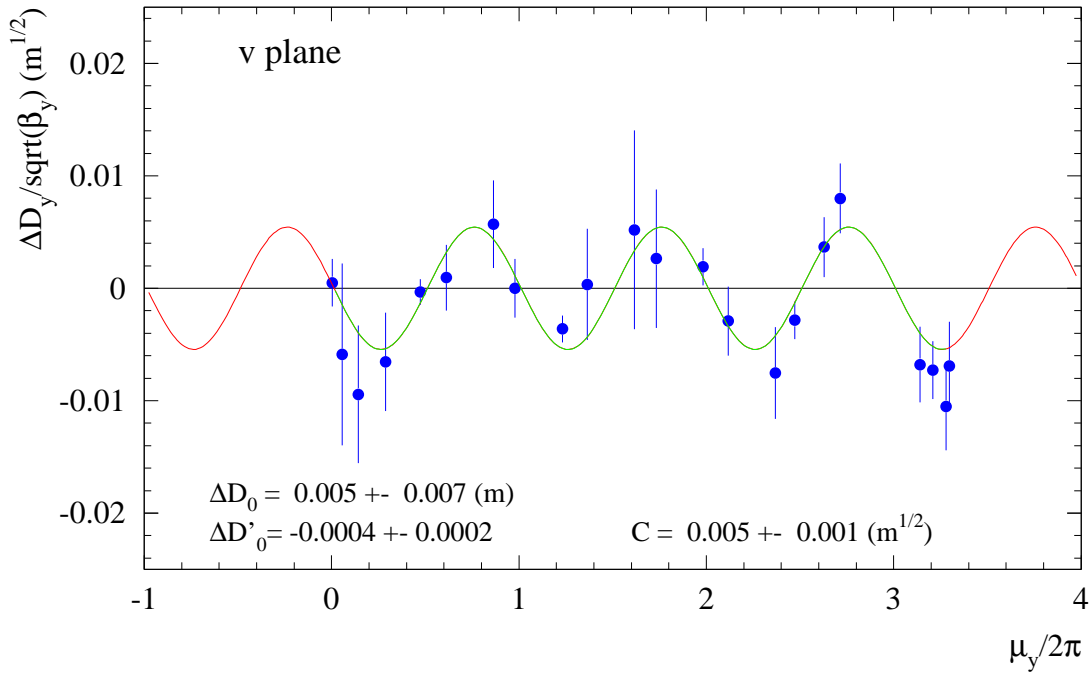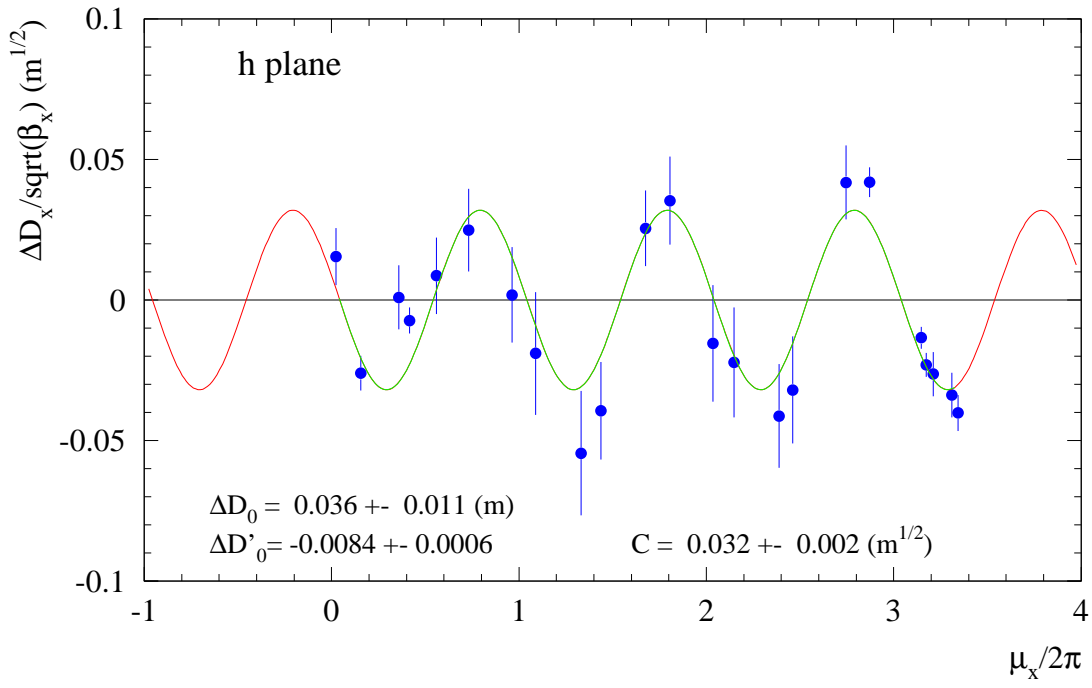
Figure 6: Fit of the dispersion error normalized to the betatron function for the horizontal (top) and vertical (bottom) plane. For this example the transfer line optics is based on the strength of fit No. 1 of Table 2.
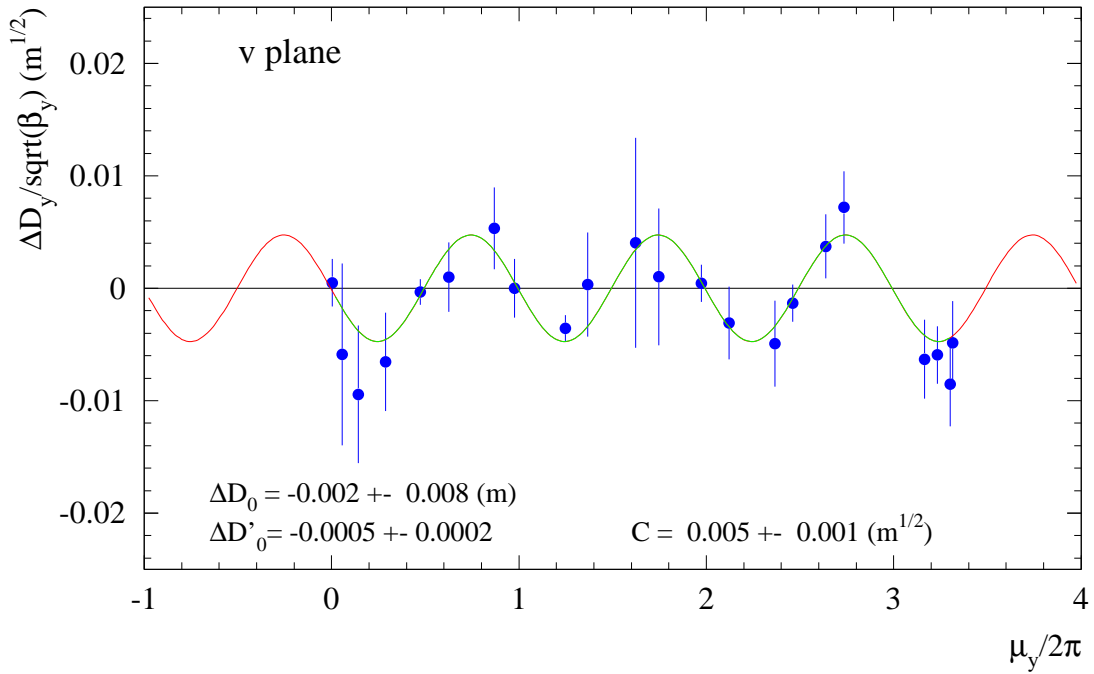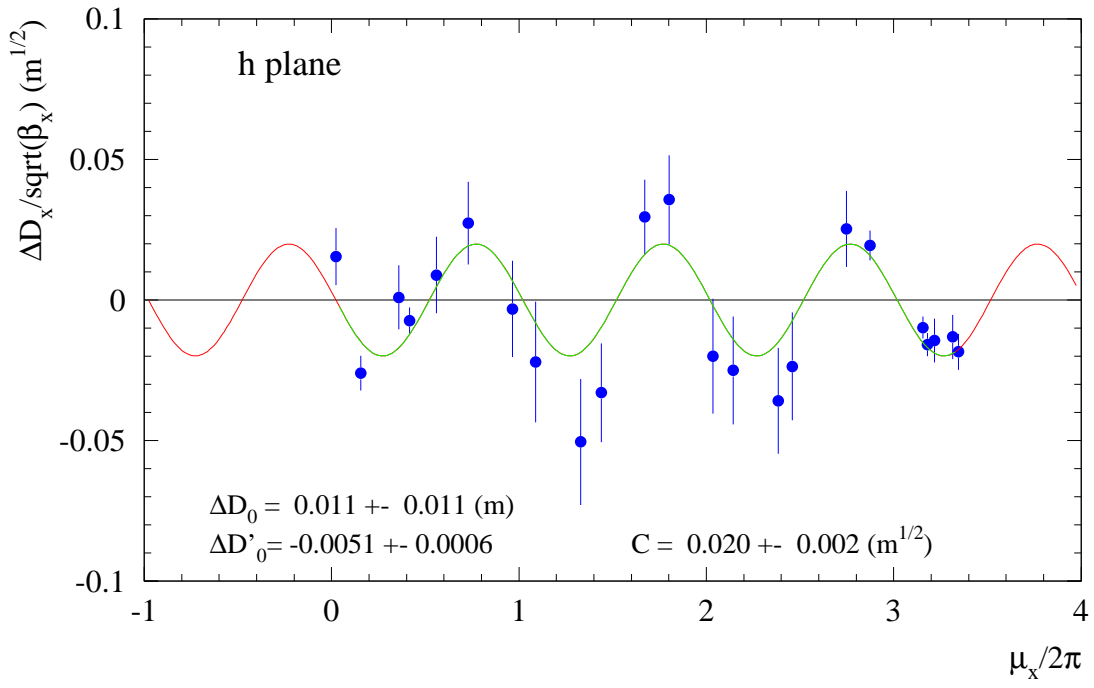
Figure 7: Fit of the dispersion error normalized to the betatron function for the horizontal (top) and vertical (bottom) plane. For this example the transfer line optics is based on the strength of fit No. 2 of Table 2.
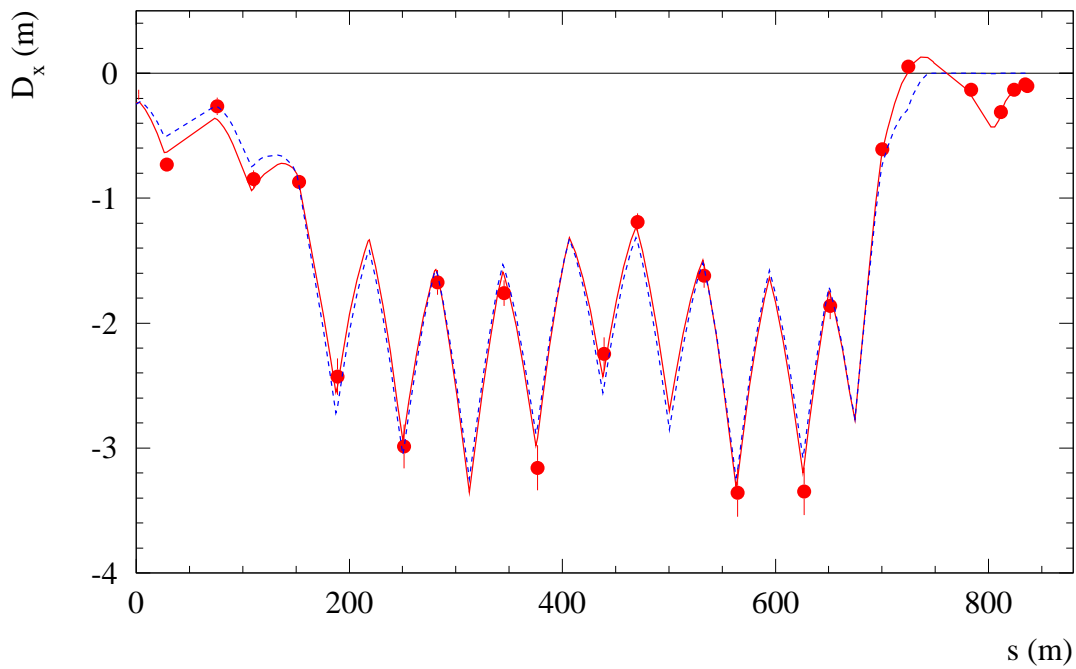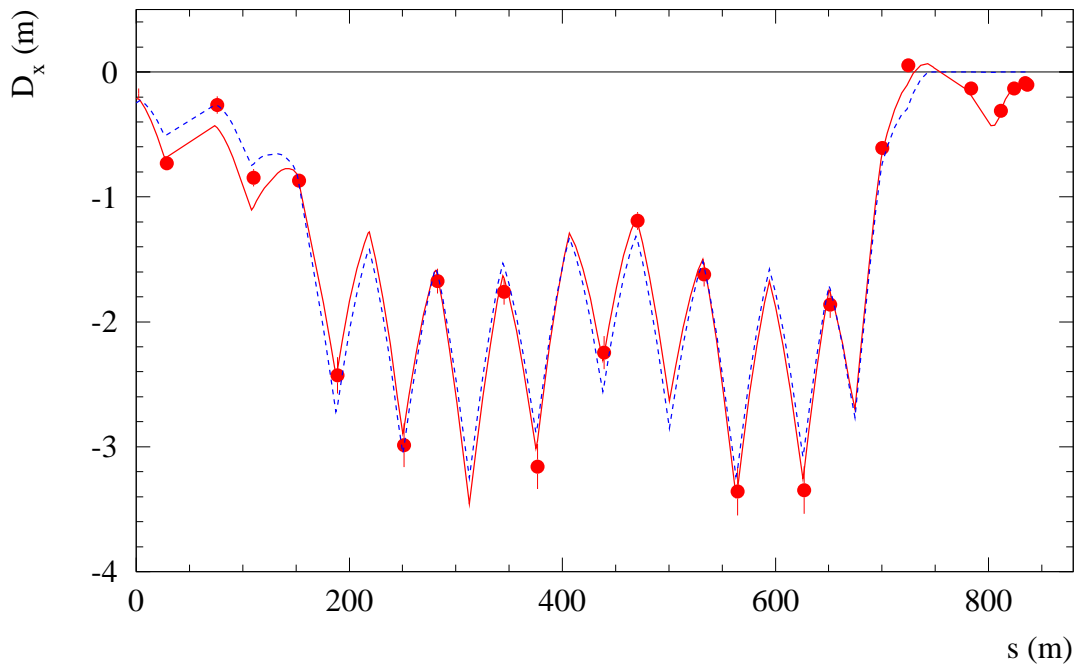
Figure 8: Fit results for the horizontal dispersion with the optics of fit No. 1 (top) and fit No. 2 (bottom). The data points and the fitted dispersion are plotted in red (point and solid line). The dashed blue line is the unperturbed dispersion. This data corresponds to the fits of Figure 6 (top) and Figure 7.
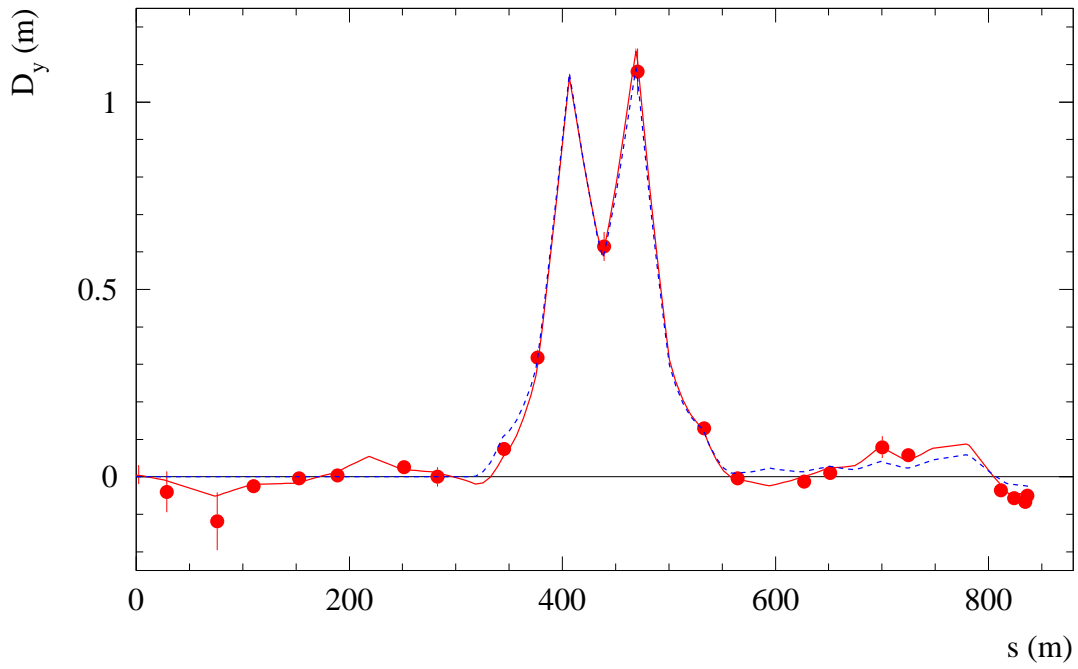
Figure 9: Fit results for the vertical dispersion with the optics of fit No. 1. The data points and the fitted dispersion are plotted in red (point and solid line). The dashed blue line is the unperturbed dispersion.

14

5 Beam Stability

During the first week-end of CNGS operation all trajectories over a period of 24 hours were recorded and analyzed. The typical intensity of the beam was in the range of 1.5×10^{13} protons per batch. 4750 good extractions were recorded and analyzed.

The trajectory sample collected during this period was analyzed using the Model Independent Analysis (MIA) approach [6, 7] which was already applied to the TI8 transfer line [5]. The idea behind this technique is to analyze large data samples to unveil correlations between measurements, for example some trajectory jitter. The basic technique in MIA is over a spatial-temporal mode analysis via a Singular Value Decomposition (SVD) of the data matrix holding the data histories. The SVD analysis decomposes the spacial and temporal variation of the beam into a superposition of orthogonal modes. Those modes are related to the underlying process that is driving the variations.

In practice the BPM trajectories are stored in a matrix A where the ith row contains the ith trajectory. The average trajectory is subtracted from the individual measurements. For convenience the matrix is normalized by a factor $(N \times M)$ where N is the number of BPMs and M the number of trajectories in the sample. The SVD algorithm decomposes a matrix A of dimension $N \times M$ into

$$A = UWV^T \tag{3}$$

where W is a $M \times M$ diagonal matrix with non-negative elements,

$$W = \begin{pmatrix} w_1 & 0 & ... & 0 \\ 0 & w_2 & & \\ ... & & ... & 0 \\ 0 & ... & 0 & w_M \end{pmatrix} \tag{4}$$

V is a $M \times M$ orthogonal matrix and U a $N \times M$ column-orthogonal matrix

$$VV^T = V^TV = 1 \qquad\qquad U^TU = 1 \tag{5}$$

This decomposition is represented schematically in Figure 10. Matrix V contains the trajectory pattern associated to each eigenvalue of W while the column vectors of matrix U describe the time evolution of the corresponding trajectory pattern. The eigenvalue indicates the amplitude of the eigenvector.

Applying this technique to the trajectory sample reveals the eigenvalue spectrum shown in Figure 11. The r.m.s. stability over 24 hours is excellent: 110 μm in the horizontal and 50 μm in the vertical plane. The horizontal spectrum contains two large eigenvalues that stand out above all others. The associated spacial vectors (resp. trajectories) are shown in Figure 12. The eigenvector associated to the largest eigenvalue corresponds to the trajectory obtained when a kick is applied at the level of the extraction septum MSE.418. The eigenvalue is therefore associated to the ripple of the septum power converter. The eigenvector corresponding to the second largest eigenvector matches the excursion obtained in case the beam is extracted with an energy error.

From the amplitude of the eigenvalues it is possible to obtain the associated r.m.s. variation of the trajectory and the corresponding ripple of the MSE.418 converter. The time evolution of the reconstructed kick is shown in Figure 13. The r.m.s. kick is $0.3\mu\mathrm{rad}$ which corresponds to
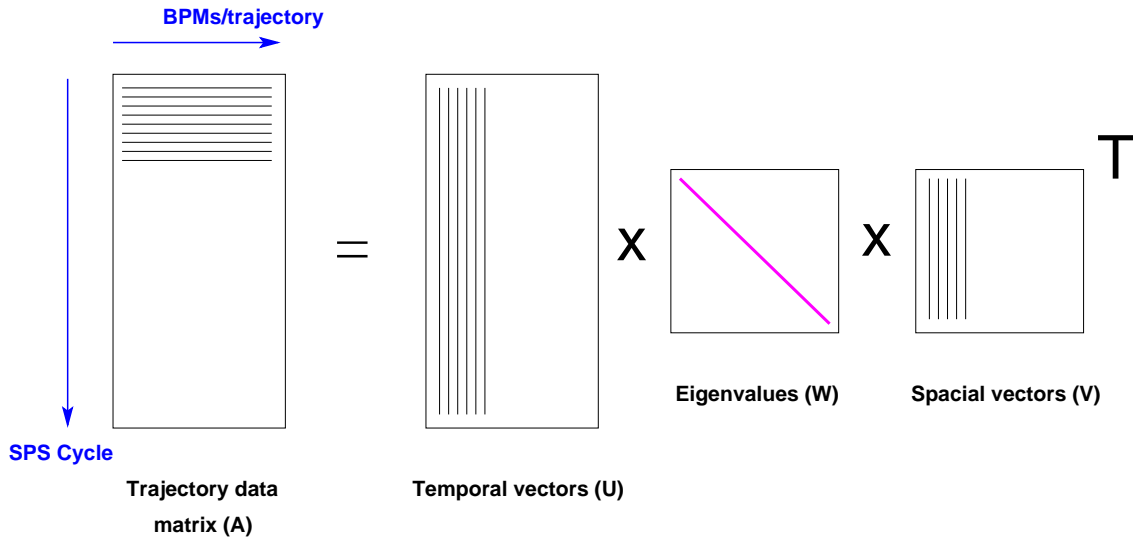
Figure 10: Schematic principle of the MIA singular value decomposition.
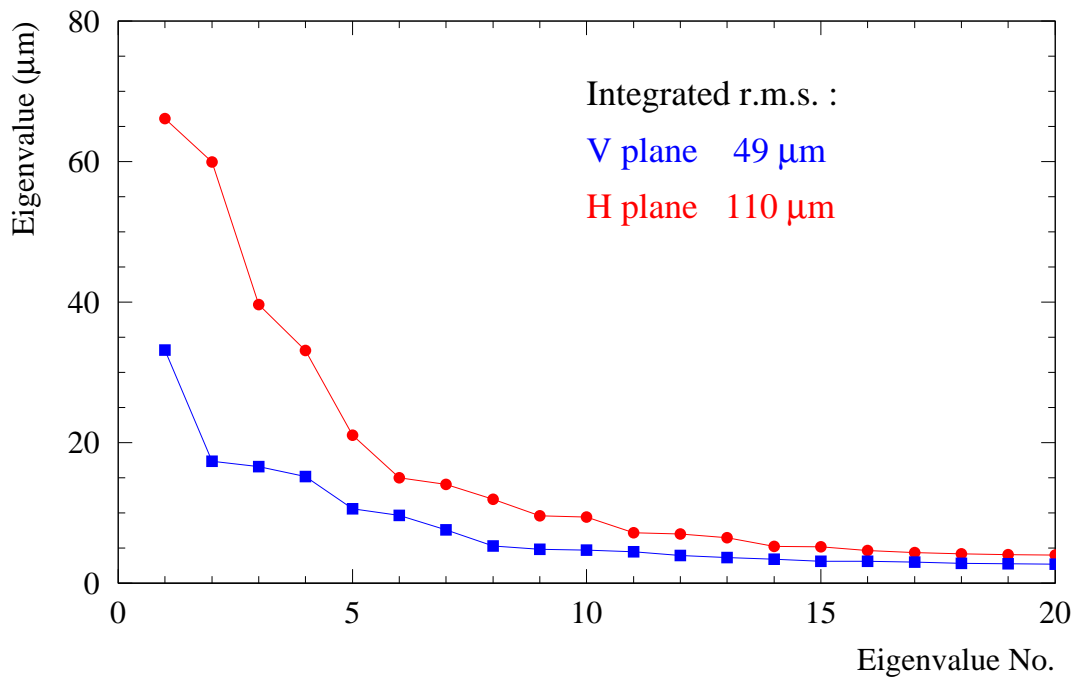

Figure 11: Spectrum of MIA eigenvalues for the horizontal and vertical planes ordered from the largest to the smallest. The quadratic sum of all eigenvalues yields the r.m.s. stability of the trajectories.
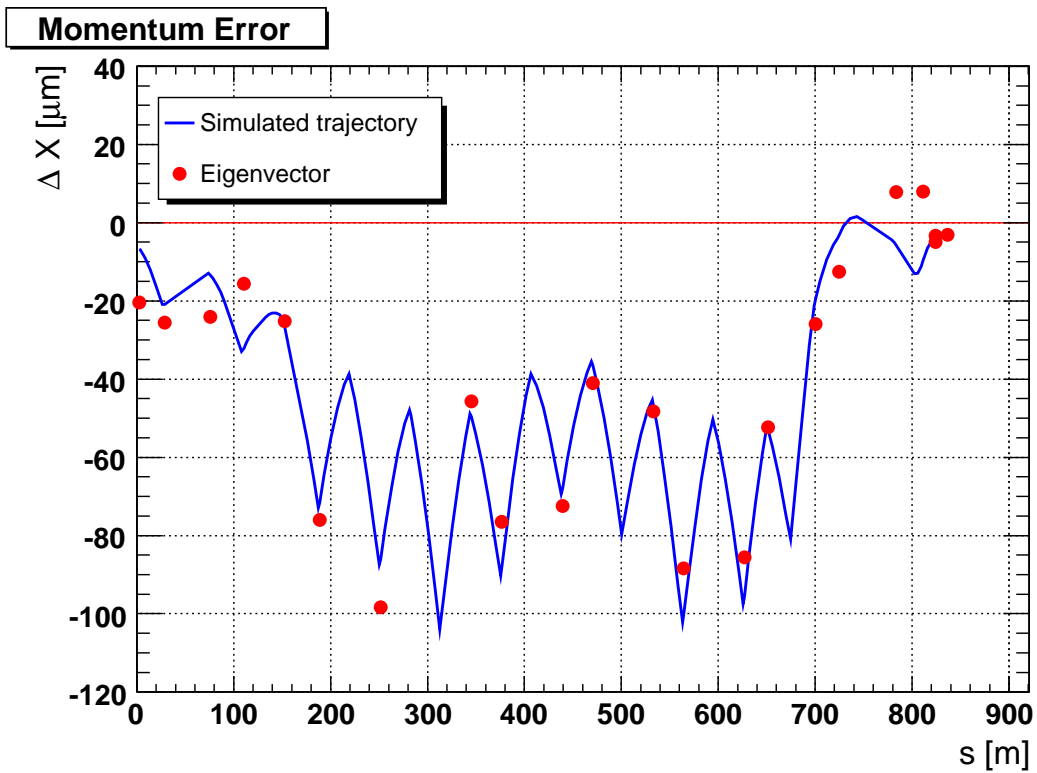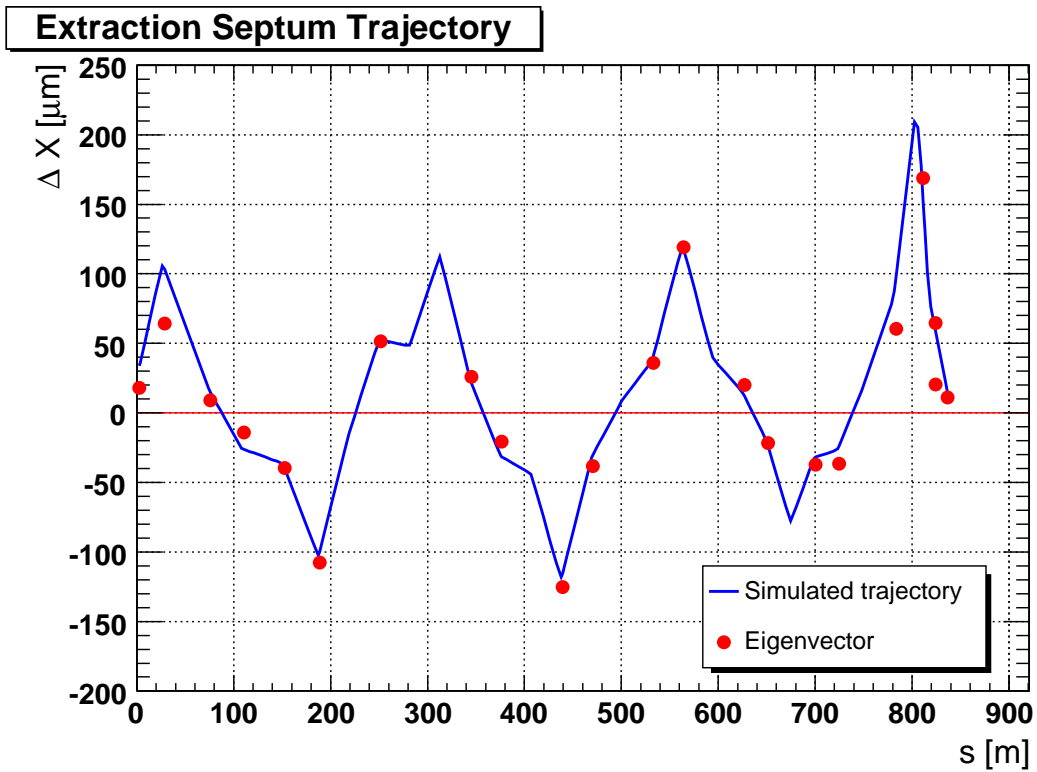
Figure 12: Spacial eigenvectors of the two largest eigenvalues in the horizontal plane. The first eigenvector corresponds to a trajectory obtained from a deflection at the MSE.418 (top). The second eigenvector corresponds to an off-energy trajectory (bottom).
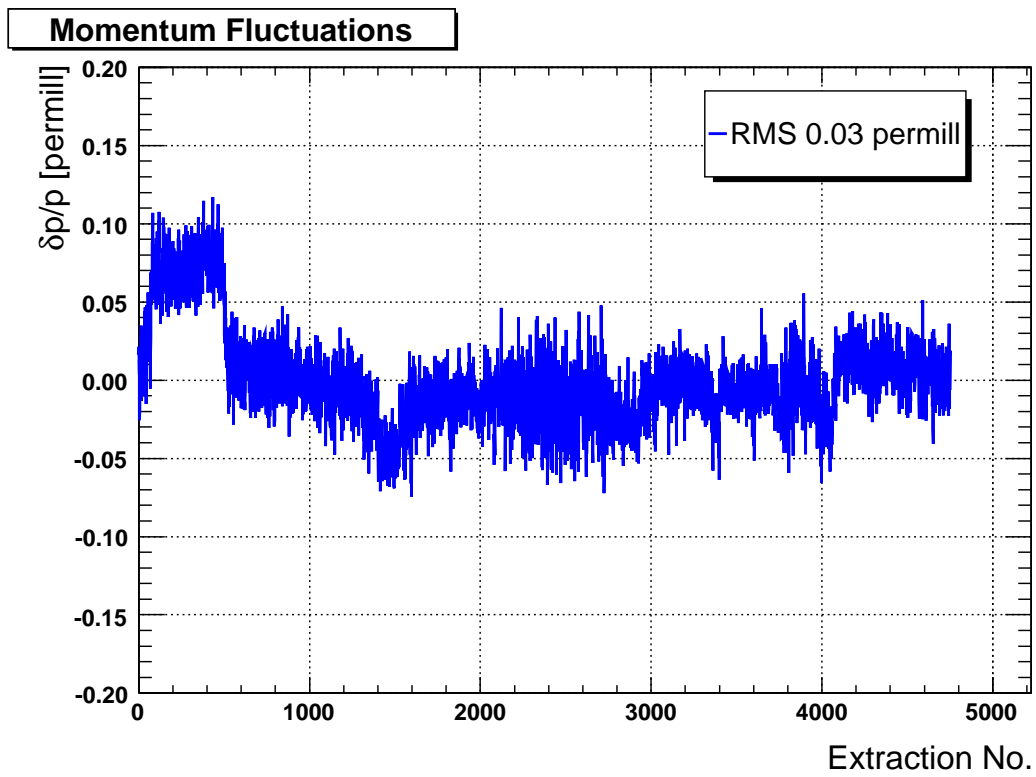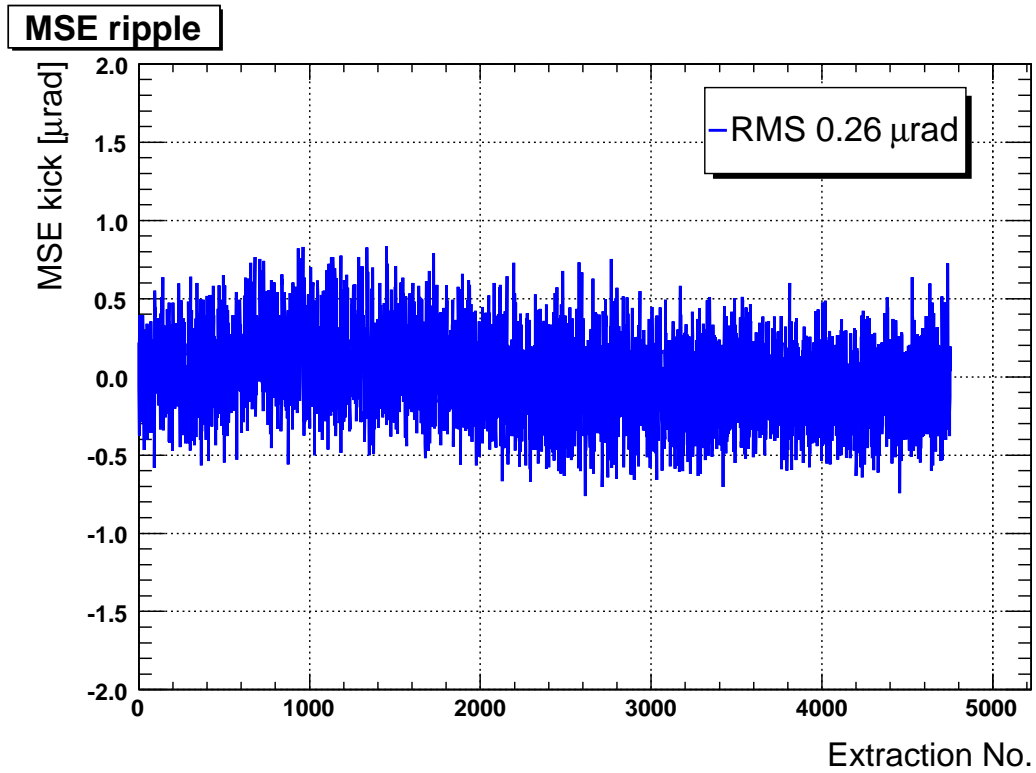
Figure 13: Time evolution of the amplitude of the two largest horizontal eigenvalues associated to the extraction septum MSE.418 (top) and to momentum fluctuations (bottom).

a ripple of 0.01%. The second largest eigenvalue corresponds to a r.m.s. energy fluctuations of 0.003%. Contrary to the case of the septum where the fluctuations seem perfectly random, the momentum fluctuations show distinct steps. Once those two largest eigenvalues are removed from the spectrum, there is no more significant difference between horizontal and vertical plane.

For all other eigenvalues, the spacial vector is mostly consistent with noise, in particular from the enlarged BPK couplers of TT40.

For the horizontal plane a change of the SPS beam momentum by $1 - 1.5 \times 10^{-4}$ is observed as the intensity is increased from 1.2×10^{13} protons per batch to 1.6^{13} protons. This is a due of the SPS radial loop based on a BPM in sextant 3 that has a small intensity dependence. Some of the momentum steps visible in Figure 13 are correlated to intensity changes of the beam in the SPS.

With such an excellent short term stability, a single trajectory correction per day using the MICADO algorithm with with 1 or 2 correctors is sufficient to maintains the r.m.s. drift below $100\ \mu$m in both planes.

Over a 10 day long period of the CNGS pilot run from, the total r.m.s. trajectory drift was 0.15 mm in the horizontal and 0.4 mm in the vertical plane. In the case of the vertical plane part of the drift actually originated in the SPS ring and was not due to changes in the transfer line itself. The excellent stability of the line is in good agreement with expectations from the analysis of the LEP orbit drift data [8].

6   Conclusion

The optics of the TT40 and TT41 transfer lines was studied and corrected during the CNGS commissioning. Response measurements revealed strength errors between 1 and 1.5% on the main quadrupole strengths that were corrected during the last week of the CNGS commissioning. The residual beta-beat from errors internal to the transfer lines is estimated to be at the level of 10% or less. The dispersion was measured and found to be very close to the nominal value. Dispersion errors coming from the SPS ring are small and do not cause significant perturbations.

The stability of the transfer line is excellent and at the level of $100\ \mu$m over 24 hours. With one trajectory correction per day it is possible to maintain the trajectory of the beam within $100\ \mu$m of the reference trajectory.

References

[1] J. Wenninger *et al.*, *Energy calibration at the SPS with Proton and Lead Ions Beams*, AB-Note-2003-014 OP.

[2] J. Wenninger, *SPS Momentum Calibration and Stability in 2003*, AB-Note-2003-091 OP.

[3] J. Safranek, Nucl. Instr. Meth. A388 (1997) 27.

[4] J. Wenninger, *Orbit Response Measurements at the SPS*, CERN-AB-2004-009.

[5] J. Wenninger, *Study of the TI 8 optics and beam stability based on beam trajectories*, AB-Note-2006-021 OP.

[6] J. Irwin *et al*, Phys. Rev. Lett 82, 1684 (1999).

[7] C. Wang, Phy. Rev. ST AB, Volume 7, 114001 (2004).

[8] R. Steinhagen, S. Raedelli and J. Wenninger, *Analysis of Ground Motion at SPS and LEP - Implications for the LHC*, CERN-AB-2005-087.